



## Nonequilibrium thermodynamic characterization of chimeras in a continuum chemical oscillator system

Premashis Kumar  and Gautam Gangopadhyay <sup>\*</sup>*S. N. Bose National Centre for Basic Sciences, Salt Lake, Kolkata 700 106, India*

(Received 7 December 2021; accepted 4 March 2022; published 21 March 2022)

The emergence of the chimera state as the counterintuitive spatial coexistence of synchronous and asynchronous regimes is addressed here in a continuum chemical oscillator system by implementing a relevant complex Ginzburg-Landau equation with global coupling. This study systematically acquires and characterizes the evolution of nonequilibrium thermodynamic entities corresponding to the chimera state. The temporal evolution of the entropy production rate exhibits a beat pattern with a series of equidistant spectral lines in the frequency domain. Symmetric profiles associated with the incoherent regime appear in descriptions of the dynamics and thermodynamics of the chimera. It is shown that identifying the semigrand Gibbs free energy of the state as the Gabor elementary function can reveal the guiding role of the information uncertainty principle in shaping the chimera energetics.

DOI: [10.1103/PhysRevE.105.034208](https://doi.org/10.1103/PhysRevE.105.034208)

### I. INTRODUCTION

The collective dynamics of systems can exhibit emergent behaviors with remarkably rich and complex features across all scales. In diverse contexts, extensive investigations have been carried out to understand these behaviors and recognize their applicability. One such emergent phenomenon that has recently received widespread scientific interest from different fields due to its intriguing and subtle nature is the chimera state [1,2]. The chimera [1,2], a counterintuitive state in the collective dynamics of coupled identical entities or continuous media [3,4], emerges as the coexistence of spatially coherent and incoherent behavior. The chimera state has received widespread scientific interest due to its intriguing and subtle nature and presence in various theoretical and experimental frameworks [5,6]. Initially, it was believed that chimeras could only exist in the array of identical phase oscillators connected by a nonlocal coupling. However, later on, evidence of amplitude-mediated chimeras [7] in the nonlocal coupling version of the complex Ginzburg-Landau equation (CGLE) [8–10] established the connection of this peculiar state to the amplitude dynamics of the system. Furthermore, the chimera state was also realized in the global (all-to-all coupling) coupling [11,12] scheme and in purely locally coupled networks [13]. All these key advancements broaden the scope of the chimera investigation into more diverse settings of collective dynamics with the main focus dedicated to a better understanding of chimera dynamics in the different coupling schemes with varied coupling strengths and various types of oscillator collections.

Nevertheless, one of the first experimental signs of chimeras was reported in a population of nonlocally coupled discrete photosensitive Belousov-Zhabotinsky chemical

oscillators [14]. In nonlocally coupled chemical oscillators [15], different variants of chimeras have been more recently demonstrated and characterized both experimentally and theoretically. However, previous works on chemical systems with global coupling have only observed oscillatory cluster patterns [16,17] or turbulent state [18]. This study aims to generate the chimera state in a simple prototypical chemical oscillator system using the global coupling scheme. The emergence of the chimera within the globally coupled framework of a chemical oscillator would complement the investigation of various possible patterns in a chemical system.

More importantly, all previous studies regarding chimera states have been limited to the dynamic aspects of the state. However, the occurrence of a similar state in neuroscience [19,20] and hydrodynamics [21,22] and possible association of the chimera with different brain states, for example, uni-hemispheric sleep [23] in different aquatic and avian species, seek a complete thermodynamic description of such a state to shed light on the basic underlying mechanisms and signatures of these similar states. A proper thermodynamic description of such emergent behaviors is still lacking. We have focused on this aspect by characterizing the chimera state in terms of thermodynamic entities. This thermodynamic investigation of a peculiar state like the chimera can broaden the current understanding of the coexistence of qualitatively different regimes and transitions among them. In this respect, knowledge of the chemical work needed to manipulate such a state and the efficiency of information spreading in the presence of the state are of crucial importance. Besides theoretical understandings, the thermodynamic picture can serve useful purposes in potential applications of such situations or exploring the real-world relevance of these states.

This study realizes the chimera state in a prototypical continuum chemical oscillator system by imposing a nonlinear globally coupled version of the CGLE and then systematically characterize the state by implementing a suitable

---

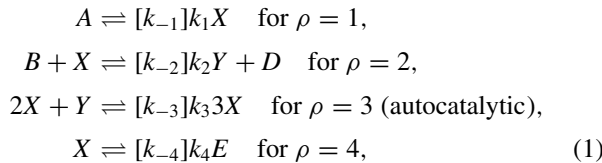
<sup>\*</sup>gautam@bose.res.in

nonequilibrium thermodynamic framework. Instead of direct incorporation of the global coupling in the reaction-diffusion system (RDS) of the Brusselator, we opt to generate the effect of coupled dynamics within the system using the modified CGLE (MCGLE) [3,11,24–26] with the global coupling at the linear and nonlinear levels. The chimera state concentration yielding the nonequilibrium nature of the system is obtained by inserting a numerically obtained amplitude from the MCGLE into an analytical equation of the concentration dynamics. Our approach thus facilitates analytically tractable thermodynamics within the nonequilibrium framework utilized here.

The layout of the paper is as follows. First, we describe the dynamics of the Brusselator reaction-diffusion system in Sec. II. In Sec. III the Brusselator system in the presence of global coupling is represented in terms of a relevant amplitude equation, and concentration fields of the intermediate species are obtained. In Sec. IV we formulate the entropy production rate and the semigrand Gibbs free energy to present the nonequilibrium thermodynamic picture. Then we provide results and a discussion in Sec. V. The paper is summarized in Sec. VI.

## II. DYNAMICS OF THE BRUSSELATOR RDS

The Brusselator model [27,28], a minimal abstract model in chemical kinetics, is capable of capturing self-sustained oscillatory behavior in the Belousov-Zhabotinsky reaction [29] and various other chemical and biological systems and has been exploited extensively to investigate many intricate and cooperative behaviors. The reversible Brusselator model is described through the chemical reactions



with  $\rho$  the reaction step label. This reaction network consists of two types of species: intermediate species with dynamic concentration  $\{X, Y\} \in I$  and externally controllable chemostated species with a constant homogeneous concentration within the timescale of interest  $\{A, B, D, E\} \in C$ . Thus, the concentration dynamics of intermediate species of the Brusselator obeys the following rate equations under the assumption that forward reaction rate constants  $k_\rho$  are much higher than reverse ones:

$$\begin{aligned} \dot{x} &= k_1a - (k_2b + k_4)x + k_3x^2y, \\ \dot{y} &= k_2bx - k_3x^2y. \end{aligned} \quad (2)$$

Here  $x = [X]$ ,  $y = [Y]$ ,  $b = [B]$ , and  $a = [A]$  are the concentrations of species. Consequently, the steady-state values of intermediate species concentration are acquired as  $x_0 = \frac{k_1}{k_4}a$  and  $y_0 = \frac{k_2k_4}{k_1k_3} \frac{b}{a}$  and the Jacobian matrix  $\mathcal{J}$  is extracted from Eq. (2) with elements  $J_{11} = -(k_2b + k_4) + 2k_3x_0y_0$ ,  $J_{12} = k_3x_0^2$ ,  $J_{21} = k_2b - 2k_3x_0y_0$ , and  $J_{22} = -k_3x_0^2$ . Now as the control parameter  $b$  is gradually varied, the Hopf instability would arise under the requirement  $J_{11} + J_{22} = 0$  at the onset and hence the critical value of the control parameter is

$b_{cH} = \frac{k_4}{k_2} + \frac{k_1^2k_3}{k_2k_4^2}a^2$ . The critical eigenvector  $U_{cH}$  corresponding to the largest eigenvalue  $\lambda_+ = i\sqrt{\frac{k_1^2k_3}{k_4}}a$  is  $U_{cH} = [1 + \frac{i}{a}\sqrt{\frac{k_4}{k_3}}\frac{1}{k_1}, -(1 + \frac{k_4^3}{k_3k_1^2}\frac{1}{a^2})]^T$ . Additionally, the critical frequency of the oscillation for Hopf instability  $f_{cH}$  can be obtained from the imaginary part of the eigenvalue at the onset of instability. Therefore, the oscillation frequency near the Hopf instability is approximately  $f_{cH} = \sqrt{\frac{k_1^2k_3}{k_4}}a$  for the Brusselator model.

After taking diffusion into account, the Brusselator RDS in one spatial dimension  $r \in [0, l]$  reads

$$\begin{aligned} \dot{x} &= k_1a - (k_2b + k_4)x + k_3x^2y + D_{11}x_{rr}, \\ \dot{y} &= k_2bx - k_3x^2y + D_{22}y_{rr}, \end{aligned} \quad (3)$$

with  $D_{11}$  and  $D_{22}$  the constant self-diffusion coefficients of intermediate species  $X$  and  $Y$ , respectively. The Jacobian matrix of the RDS in Eq. (8) is  $\mathcal{J}_{\mathcal{D}} = \mathcal{J} - q^2\mathcal{D}$ , with  $q$  the wave number. In the presence of diffusion, the onset of Hopf instability demands  $\text{Tr}(\mathcal{J}_{\mathcal{D}}) = 0$ , and hence the critical value of the control parameter  $b$  is specified as  $b_{ctw} = \frac{k_4}{k_2} + \frac{k_1^2k_3}{k_2k_4^2}a^2 + \frac{D_{11}+D_{22}}{k_2}q^2$ , where the wave number  $q = \frac{2n\pi}{l}$  according to periodic boundary conditions in the finite domain  $l$ , with  $n$  an integer. However, to restrict our investigation solely to the Hopf instability regime, we set the wave number  $q = 0$  here.

## III. BRUSSELATOR REPRESENTATION WITH GLOBAL COUPLING

The amplitude dynamics encapsulates the essential role of nonlinearity in pattern formation [10]. For a nonlinear chemical system like the Brusselator, the concentration dynamics of the intermediate species can be acquired by exploiting the amplitude as the multiplicative factor in the standard linear stability description of the system. Here we consider that a globally coupled system of Brusselators can be effectively represented in terms of the amplitude of the MCGLE near the onset of Hopf instability since the amplitude of the CGLE guides the reaction-diffusion dynamics near the Hopf bifurcation point by capturing crucial nonlinear features of the system. The normal form of the CGLE [10,30] in a spatially extended system can be expressed as

$$\frac{\partial Z}{\partial t} = \lambda Z - (1 - i\beta)|Z|^2Z + (1 + i\alpha)\partial_r^2Z, \quad (4)$$

with  $Z$  the amplitude field and  $\lambda$ ,  $\beta$ , and  $\alpha$  coefficients encompassing the details of a particular system. In the presence of a global coupling, the normal form of the CGLE (4) can be recast into the MCGLE [24,25]

$$\begin{aligned} \frac{\partial Z}{\partial t} &= \lambda Z - (1 - i\beta)|Z|^2Z + (1 + i\alpha)\partial_r^2Z \\ &\quad - (\lambda + i\nu)\langle Z \rangle + (1 - i\beta)\langle |Z|^2Z \rangle, \end{aligned} \quad (5)$$

where  $\langle \dots \rangle$  denotes the spatial average. Now the spatial average over Eq. (5) yields an oscillatory mean field  $\langle Z \rangle = Z_0 = \eta \exp(-i\nu t)$ , with  $\eta$  and  $\nu$  the amplitude and the frequency of the oscillation, respectively. This mean-field oscillation is a feature of the nonlinear global coupling of the MCGLE. By substituting  $Z = Z_0(1 + Z_{IH})$ , with an arbitrary

inhomogeneity  $Z_{IH}$ , into Eq. (5) followed by a linear stability analysis, we can determine the threshold value of the  $\eta$  as  $\eta_c = \sqrt{\frac{\lambda}{2}}$ , below which uniform oscillation becomes unstable irrespective of other parameter values. Further, the coefficients  $\alpha$  and  $\beta$  are obtained by implementing the Krylov-Bogoliubov averaging method [31,32] to the normal form of the CGLE. For the Brusselator, the coefficients are acquired as  $\alpha = \frac{\Omega(D_{22}-D_{11})}{D_{11}+D_{22}}$ ,  $\beta = \frac{p_2}{p_1} \frac{1}{3a}$ , and  $\lambda = \frac{b-1-a^2}{2}$ , with the ratio of correction factors  $\frac{p_1}{p_2}$  being  $\frac{4-7a^2+4a^4}{2+a^2}$ . For the investigation of the chimera state, we set  $\eta = 0.66\sqrt{\lambda}$  and  $\nu = \frac{\lambda}{10}$  throughout the paper.

To acquire the amplitude in the presence of the global coupling, we solve Eq. (5) numerically using a pseudospectral method including an exponential time differencing algorithm [33]. For the purpose of simulation, we exploit a computational time step of 0.01 and consider 2048 grid points for the spatial domain used in this investigation. As an initial state of the system, a uniform state with additional noise is chosen. We apply periodic boundary conditions. In the numerical simulation, all coefficients of Eq. (5) are specified in terms of parameters of the Brusselator in Eq. (8). On combining the numerically obtained amplitude field with a linear stability description of the nonlinear system, the collective concentration dynamics of the Brusselator system is acquired through the equation

$$z_{IH} = z_{I0} + A_M U_{cH} \exp(i f_{cH} t) + \text{c.c.}, \quad (6)$$

with  $A_M$  the numerically derived amplitude field from Eq. (5),  $z_{I0}$  the initial uniform concentration field set by steady-state values of two intermediate species, and  $f_{cH} = \sqrt{\frac{k_2^2 k_3}{k_4}} a$  the critical frequency of the Brusselator within the Hopf instability regime. Here the chimera state arises in the chemical system in the presence of global coupling and we consider this coupling to be present at the level of amplitude dynamics only. Thus incorporation of the numerically obtained amplitude with the linear stability representation of the Brusselator system would illustrate the essential feature of the chimera in the concentration dynamics.

#### IV. NONEQUILIBRIUM THERMODYNAMIC DESCRIPTION

We have employed a recently developed nonequilibrium thermodynamic framework [34,35] to capture the entropic and energetic description of the chimera state. Incorporation of the nonequilibrium steady-state representation with the MCGLE scheme makes the thermodynamic description of the collective system possible.

##### A. Entropy production rate

The entropy production rate (EPR) due to the chemical reaction can be derived by utilizing the flux-force form in which fluxes obey the mass action law  $j_{\pm\rho} = k_{\pm\rho} \prod_{\sigma} z_{\sigma}^{v_{\pm\rho}^{\sigma}}$ , where  $+$  and  $-$  denote the forward and backward reactions, respectively, and the force is the affinity of the reaction [36]  $f_{\rho} = -\sum_{\sigma} S_{\rho}^{\sigma} \mu_{\sigma}$ , with  $S_{\rho}^{\sigma} = v_{\rho}^{\sigma} - v_{+\rho}^{\sigma}$  the stoichiometric coefficient of species and  $\mu_{\sigma}$  the chemical potential. For the

solvent concentration  $z_0$  and the standard-state chemical potential  $\mu_{\sigma}^o$ , the chemical potential is given as  $\mu_{\sigma} = \mu_{\sigma}^o + \ln \frac{z_{\sigma}}{z_0}$ . Thus, the entropy production rate due to the chemical reaction is given as  $\frac{dS_R}{dt} = \frac{1}{T} \int dr \sum_{\rho} (j_{+\rho} - j_{-\rho}) \ln \frac{j_{+\rho}}{j_{-\rho}}$ , with affinities expressed in terms of the reaction fluxes  $f_{\rho} = \ln \frac{j_{+\rho}}{j_{-\rho}}$  and  $T$  the constant absolute temperature set by solvent. Similarly, the diffusive flux and affinity represent the entropy production rate due to diffusion as  $\frac{dS_D}{dt} = \int dr [D_{11} \frac{\|\frac{\partial x}{\partial r}\|^2}{x} + D_{22} \frac{\|\frac{\partial y}{\partial r}\|^2}{y}]$ , with the total entropy production rate comprised of the reaction entropy production rate and diffusion entropy production rate.

##### B. Semigrand Gibbs free energy

Now the stoichiometric matrix of the chemical reaction network in Eq. (1) is

$$S_{\rho}^{\sigma} = \begin{matrix} & R_1 & R_2 & R_3 & R_4 \\ \begin{matrix} X \\ Y \\ A \\ B \\ D \\ E \end{matrix} & \begin{pmatrix} 1 & -1 & 1 & -1 \\ 0 & 1 & -1 & 0 \\ -1 & 0 & 0 & 0 \\ 0 & -1 & 0 & 0 \\ 0 & 1 & 0 & 0 \\ 0 & 0 & 0 & 1 \end{pmatrix} \end{matrix}. \quad (7)$$

In a closed system, conservation laws [37] are specified as the left null vectors corresponding to the left null space of the stoichiometric matrix  $\sum_{\sigma} l_{\sigma}^{\lambda} S_{\rho}^{\sigma} = 0$ , where  $\{l_{\sigma}^{\lambda}\} \in \mathbb{R}^{(\sigma-w) \times \sigma}$ , with  $w = \text{rank}(S_{\rho}^{\sigma})$ . Components, i.e., globally conserved quantities of the reaction network, can be constituted using conservation laws as  $L_{\lambda} = \sum_{\sigma} l_{\sigma}^{\lambda} z_{\sigma}$  such that  $\frac{d}{dt} \int dr L_{\lambda} = 0$ . For the stoichiometric matrix in Eq. (7), the conservation laws of the closed reaction network are acquired as two linearly independent  $1 \times 6$  vectors  $l_{\sigma}^{\lambda=1} = (1 \ 1 \ 1 \ 0 \ 0 \ 1)$  and  $l_{\sigma}^{\lambda=2} = (0 \ 0 \ 0 \ 1 \ 1 \ 0)$ . Hence, the corresponding components are expressed as  $L_1 = x + y + a + e$  and  $L_2 = b + d$ . A conservation law can be broken when a closed system is opened by chemostating. Therefore, conservation laws in an open system are generally characterized as  $\{l^{\lambda}\} = \{l^{\lambda_b}\} \cup \{l^{\lambda_u}\}$  and the set of chemostated species can be divided into two subsets  $\{C\} = \{C_b\} \cup \{C_u\}$ , with labels  $u$  and  $b$  denoting unbroken and broken ones, respectively. Here both conservation laws of the Brusselator model can be broken by chemostated species  $A$  and  $B$ . Therefore, the pair of  $A$  and  $B$  belongs to the set  $C_b$  and is considered as the reference chemostated species here.

In terms of the chemical potential, the nonequilibrium Gibbs free energy of a reaction network is defined as [38]  $G = G_0 + \sum_{\sigma \neq 0} (z_{\sigma} \mu_{\sigma} - z_{\sigma}^o)$ , with  $G_0 = z_0 \mu_0^o$ . However, the Gibbs free energy does not represent the proper energetics of the system operating far from equilibrium. To capture the proper energetics of the chimera, we need to employ the semigrand Gibbs free energy obtained by the Legendre transformation of the nonequilibrium Gibbs free energy [34,35]

$$\mathcal{G} = G - \sum_{\lambda_b} \mu_{\lambda_b} M_{\lambda_b}, \quad (8)$$

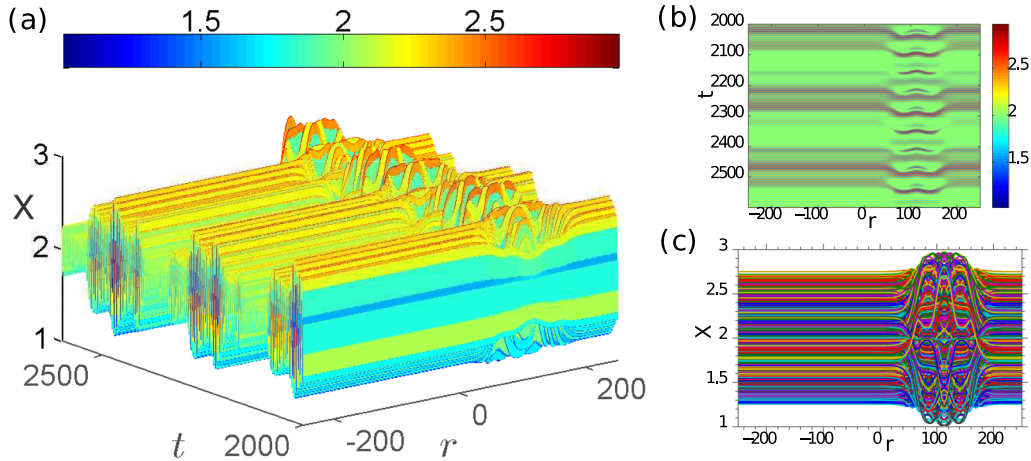


FIG. 1. (a) Three-dimensional concentration field and (b) corresponding space-time image of the activator in the Brusselator system. (c) Concentration dynamics along the spatial axis. The concentration dynamics is explicitly assessed from Eq. (6) by exploiting the 2001 amplitude snapshots between times  $t = 2000$  and  $t = 2600$ . For the simulation of the related MCGLE, we use a time-step size of 0.01 and divide the one-dimensional system length  $l = 500$  into 2048 grid points, starting from a uniform state at  $t = 0$ . All illustrations are obtained for  $D_{11} = 4$ ,  $D_{22} = 3.2$ ,  $l = 500$ ,  $a = 2$ ,  $b = 5.28$ , and  $k_{-\rho} = 10^{-4} \ll k_{\rho} = 1$ .

with  $M_{\lambda_b} = \sum_{C_b} l_{C_b}^{\lambda_b-1} L_{\lambda_b}$  the moieties [39] exchanged between chemostats and the system.

## V. RESULTS AND DISCUSSION

The spatiotemporal evolution of the activator concentration of the system is depicted in Fig. 1. Initially, the system is kept at a uniform base state. The chimera concentration dynamics is obtained from Eq. (6) by using the 2001 amplitude snapshots between times  $t = 2000$  and  $t = 2600$ . For the simulation of the MCGLE, we consider a time-step size of 0.01 and divide the one-dimensional system of length  $l = 500$  into 2048 grid points. All illustrations are obtained for diffusion coefficients  $D_{11} = 4$  and  $D_{22} = 3.2$ , chemostated concentrations  $a = 2$  and  $b = 5.28$ , and chemical reaction rate constants  $k_{-\rho} = 10^{-4} \ll k_{\rho} = 1$ . The appearance of the chimera state in the three-dimensional concentration field of the activator can be observed in Fig. 1(a). The corresponding space-time realization of the chimera is presented in Fig. 1(b). The image shows an embedded incoherent regime within the coherent counterparts of the state. The incoherent nature of the activator concentration field is apparent in Fig. 1(c) with the turbulent concentration around  $r \approx 100$ . It is also realized from the concentration field that the coherent region evolves with time. We acquire the space-integrated concentration  $X_s$  and time-integrated concentration  $X_m$  from the spatiotemporal concentration field of intermediate species  $X$  in Eq. (6) by taking the summation over the spatiotemporal concentration data along the spatial length and temporal domain, respectively. The temporal evolution of the space-integrated concentration  $X_s$  in Fig. 2(a) reveals a beat interference pattern with a periodic envelope of the temporal profile. A similar beat phenomenon in the chemical system of periodically forced pH oscillator [40] has been reported recently. We assert that the emergence of a beat pattern in the temporal domain of the chimera state is associated with the global coupling scheme of the amplitude equation. The temporal trait of the entropy

production rate in Fig. 2(b) seemingly reflects qualitatively the same behavior as the space-integrated concentration in Fig. 2(a). However, in Fig. 2(c) the power spectrum of the space-integrated concentration has two lines, whereas the EPR power spectrum exhibits a series of equidistant spectral lines with gradually decreasing power in the frequency domain. These frequencies related to the spectral lines are determined by a center frequency  $f_o$  and spacing between consecutive lines  $\delta f$  as  $f_n = n(\delta f) + f_o$ , with  $n$  an integer. This feature in the frequency domain of the entropy production rate is generated due to the underlying mixing of frequency components of concentrations in the entropy production rate representation and the intrinsic nonlinearity of the system. The generation of new frequencies is evident from the emergence of an additional frequency line in the power spectrum of the space-integrated  $X^2$ . Power spectra in Fig. 2(c) are obtained by implementing Welch's power spectral density estimate [41] using a Hann window and an adequate discrete Fourier transform length in MATLAB.

Now the time-integrated activator concentration in Fig. 2(d) and the spatial EPR in Fig. 2(e) have an even-symmetric structure corresponding to the incoherent state of the chimera in an otherwise flat profile associated with the coherent regimes. This symmetry of the incoherent state in dynamic and thermodynamic entities is possibly inherited from the uniform nature of the global coupling. The time-integrated concentration has a composite pulse structure in the incoherent regime with an increased concentration at the axis of symmetry. Away from the axis, the principal concentration peak of the pulse subsides into a secondary peak preceded by a notch on both sides. The incoherent state in the spatiotemporal realization of the chimera can be visualized as the inclusion of strong spatial amplitude fluctuation over time to this symmetric time-integrated profile. The spatial EPR in Fig. 2(e) exhibits a symmetric double-hump structure with a global minimum associated with the peak in the time-integrated concentration. The hump in this EPR profile is related to the secondary peak in the concentration profile and



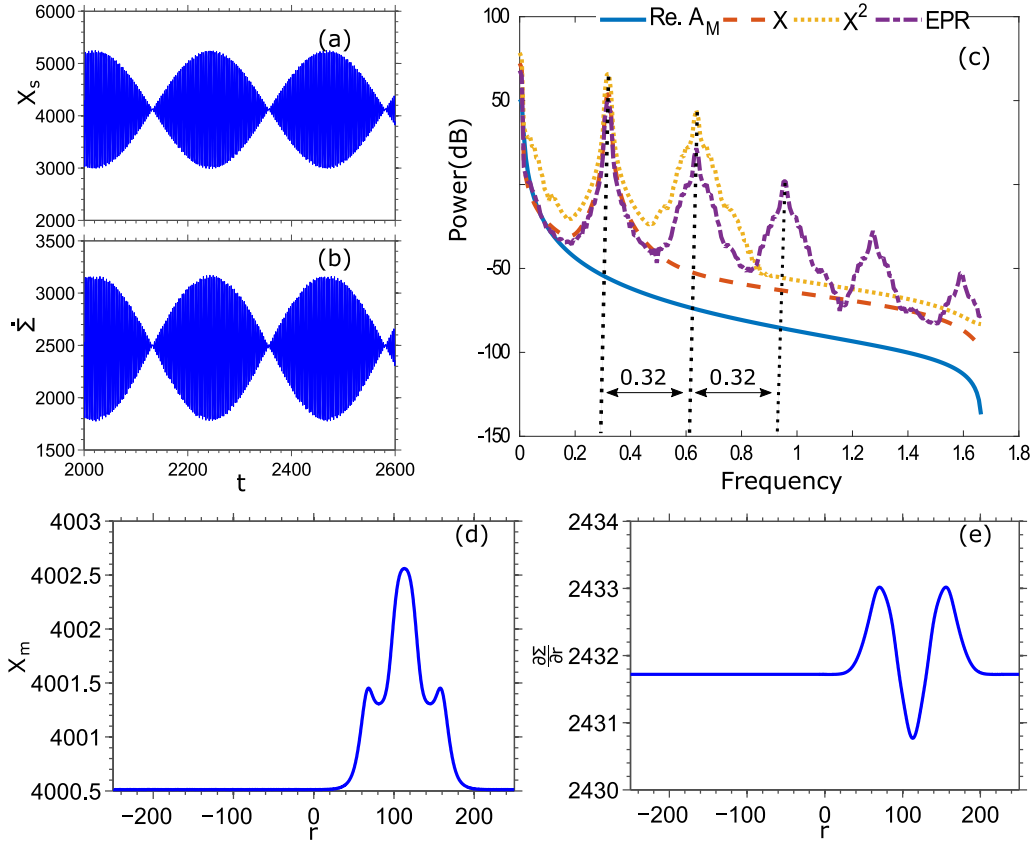


FIG. 2. (a) Space-integrated concentration  $X_s$  variation with time shows a beat interference pattern. (b) The behavior of the EPR is qualitatively similar to the temporal dynamics of the global concentration. (c) Power spectrum of the space-integrated amplitude, concentration, and EPR. For the power spectrum, we implement Welch's power spectral density estimate using a Hann window. (d) Time-integrated concentration  $X_m$  over the spatial axis. (e) Spatial EPR. In (d) and (e) the incoherent state can be identified as symmetric profiles. Here the space-integrated concentration  $X_s$  and time-integrated concentration  $X_m$  are obtained by taking the sum over the spatiotemporal concentration field of intermediate species  $X$  along the spatial length and temporal domain, respectively. For chemostated species the concentrations are set at  $b = 5.28$ ,  $a = 2$ , and  $d = e = 10^{-4}$ , with  $d$  and  $e$  denoting the concentrations of  $D$  and  $E$ , respectively.

acts as a marker for the transition from the incoherent to the coherent regime. Hence, the transition between the coherent and incoherent regimes causes the largest spatial increase in dissipation. This kind of regular structure corresponding to the incoherent state of the chimera is reminiscent of the previously demonstrated highly ordered time-average states of the chaotic spatiotemporal pattern [42].

Figure 3(a) demonstrates that the semigrand Gibbs free energy of the chimera state is always greater than its homogeneous counterpart as they are connected by a non-negative relative entropy of concentration distributions [35]. The homogeneous counterpart is related to a uniform concentration field of the system set by steady-state values of intermediate species. The nature of the transition among coherent and incoherent states in chimeras is quite apparent in terms of the energetics of the system illustrated through the semigrand Gibbs free energy profile and its spatial gradient in Figs. 3(a) and 3(b), respectively. More specifically, a notch on both sides marks the transition from the coherent to the incoherent state and this notch is generated due to the previously mentioned maximum spatial dissipation rate during the transition. Additionally, the core of the incoherent state in this chimera is identified by a symmetric peak which hints at the lower

energetic stability of the incoherent state than its coherent counterpart.

More interestingly, we identify that the semigrand Gibbs free energy characteristics of the chimera render a one-dimensional Gabor elementary function (GEF) [43] described as a Gaussian-modulated complex exponential function  $\exp(-\frac{r^2}{2\tilde{w}^2} - i\tilde{k}r)$ , with the standard deviation  $\tilde{w}$  of the Gaussian envelope and preferred wave number  $\tilde{k}$ . Thus, the semigrand Gibbs free energy here can be equivalently expressed in terms of a scaled and translated improved family of the Gabor elementary function as  $\mathcal{G} \equiv \mathcal{G}_c + Q \exp[-\frac{(r-r_0)^2}{2\tilde{w}^2} - i\tilde{k}(r-r_0)]$ , where  $Q$  is the scaling factor,  $r_0$  is the location of the center, and  $\mathcal{G}_c$  is the semigrand Gibbs free energy of coherent regimes acting as the shift factor. The family of Gabor elementary functions in the above expression maintains the lowest possible bound of joint uncertainty in space and wave number  $\sigma_r \sigma_k = \frac{1}{2}$ .

Due to the even symmetry of the semigrand Gibbs free energy characteristics in Fig. 3(a), the real component of the one-dimensional Gabor elementary function with a suitable choice of parameters provides a reasonable fit to the semigrand Gibbs free energy profile as shown in Fig. 3(c). The

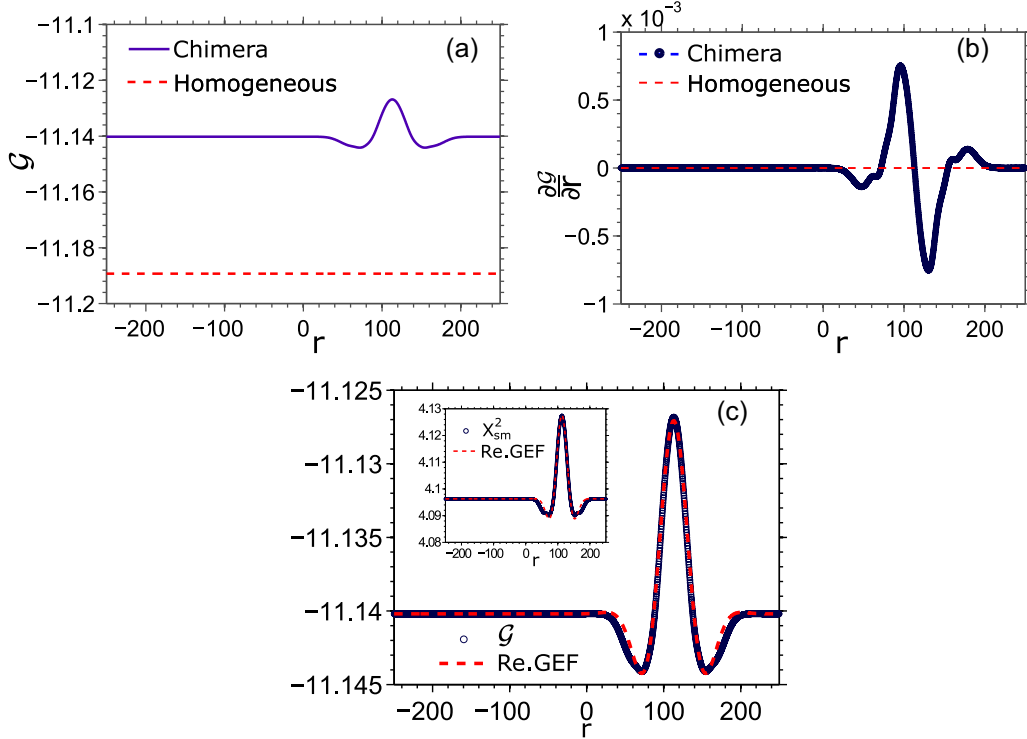


FIG. 3. (a) Semigrand Gibbs free energy of the chimera state (solid blue line) and (b) corresponding slope (blue line with circle) compared to the same entities for the homogeneous state (red dashed line). The homogeneous counterpart refers to a uniform field set by steady-state values of intermediate species. (c) Real part of the GEF fit to the semigrand Gibbs free energy. A chemostated species pair ( $A$  and  $B$ ) is considered as the reference chemostated species. All the parameters are the same as in Fig. 1.

intriguing agreement of the chimera energetics with the Gabor elementary function allows one to exploit the interpretability of the Gabor elementary function to predict and manipulate the information transmitting capacity of the chimera over a given spatial domain. For example, one can readily say that Gabor's uncertainty principle [43–45] for information regarding localization trade-off in two conjugate domains is also equally valid for the semigrand Gibbs free energy of the chimera state. Moreover, the association of the semigrand Gibbs free energy with the Gabor elementary function also means that different chimera energy profiles in separate parametric regimes can be generated by dilation and translation of a particular Gabor elementary function related to a specific semigrand Gibbs free energy structure. Thus, corresponding to the energetic responses of chimera states at various control parameter values, we identify a different preferred wave number  $\tilde{k}$ , center location  $r_0$ , scaling factor  $Q$ , and Gaussian envelope width  $\tilde{k}$  (see Table I) of Gabor elementary functions having spatial wave-number localiza-

TABLE I. Joint uncertainty metric of the real  $(\sigma_r\sigma_k)_c$  and imaginary  $(\sigma_r\sigma_k)_s$  components of the Gabor elementary function for different values of the control parameter  $b$ .

$b$	$\mathcal{G}_c$	$(Q, \tilde{w})$	$(r_0, \tilde{k})$	$(\sigma_r\sigma_k)_c$	$(\sigma_r\sigma_k)_s$
5.24	-11.11	(0.011, 37.50)	(137.70, 0.063)	2.36	2.46
5.28	-11.14	(0.013, 30.79)	(113.04, 0.060)	1.68	2.14
5.32	-11.17	(0.017, 30.50)	(112.30, 0.0485)	1.14	2.00
5.38	-11.21	(0.024, 27.50)	(111.82, 0.043)	0.82	1.90

tion trade-offs. Interestingly, it is evident from Table I that, unlike the whole Gabor elementary function case, the real and imaginary components of Gabor elementary functions have a Gaussian width-dependent joint uncertainty metric that can serve as an independent marker of chimera energetics.

The Gabor representation of chimera energetics reveals the role of the constraint set by the uncertainty principle of information in shaping the thermodynamic evolution of the system. Besides these, the Gabor elementary function quantification of the time-integrated chimera dynamics provides crucial knowledge about evaluating the chimera state from an information-theoretic viewpoint; for example, the wave-number selectivity for the coherent profile can be estimated from the center wave number  $\tilde{k}$  of the Gabor elementary function fitted to the time sample-averaged  $X^2$  [inset in Fig. 3(c)].

## VI. CONCLUSION

To sum up, our work has captured the emergence of the chimera within a globally coupled continuum chemical oscillatory system and presented the corresponding nonequilibrium thermodynamic signatures. On this basis, we have identified the association of the chimera energetics with the Gabor representation having the minimum theoretically possible joint uncertainty metric. Our demonstration of beat characteristics in the temporal rate of entropy production and the symmetric profiles of spatial entropy production in this study could be treated as key diagnostic elements to detect the nature of chimeras under different coupling schemes and

diverse collective systems. In this regard, the thermodynamic characterization of the chimera could be extended to the traditional chimera in a ring of nonlocally coupled oscillators [46] or multichimera states resulting from strong nonlinear coupling [47]. The thermodynamic insight of the chimera state could also be applicable in the investigation of the connection between the chimera state and synchronous state in Kuramoto-type networks [48]. For instance, these thermodynamic signatures can be utilized to qualitatively differentiate the chimera from other symmetry-breaking phenomena of such networks. Hence, detailed comparative studies of the entropic and energetic signature for various chimera classes [5,49] need to be carried out.

Moreover, rendering the energy characteristics of the chimera in terms of the Gabor representation here would complement the information thermodynamic [35] aspect of the pattern formation. The Gabor correspondence of the chimera

energetics would immensely aid in accessing the similarity of the chimera with various other seemingly analogous states [19–22] and thus provide crucial insight into the understanding of the general spatial pattern of partial synchrony. The thermodynamic quantification of the chimera and its information-theoretic connection conferred here can enhance the efficiency of a chimera-based architecture [50] and may present application possibilities of the state outside the laboratory, from image representation [51,52] to the representation of the primary visual system [53].

#### ACKNOWLEDGMENT

P.K. acknowledges fruitful discussions with Katharina Krischer and Sindre W. Haugland concerning numerical aspects of chimera states.

- 
- [1] Y. Kuramoto and D. Battogtokh, Coexistence of coherence and incoherence in nonlocally coupled phase oscillators, *Nonlinear Phenom. Complex Syst.* **5**, 380 (2002).
- [2] D. M. Abrams and S. H. Strogatz, Chimera States for Coupled Oscillators, *Phys. Rev. Lett.* **93**, 174102 (2004).
- [3] L. Schmidt and K. Krischer, Chimeras in globally coupled oscillatory systems: From ensembles of oscillators to spatially continuous media, *Chaos* **25**, 064401 (2015).
- [4] Z. G. Nicolaou, H. Riecke, and A. E. Motter, Chimera States in Continuous Media: Existence and Distinctness, *Phys. Rev. Lett.* **119**, 244101 (2017).
- [5] F. Parastesh, S. Jafari, H. Azarnoush, Z. Shahriari, Z. Wang, S. Boccaletti, and M. Perc, Chimeras, *Phys. Rep.* **898**, 1 (2021).
- [6] S. W. Haugland, The changing notion of chimera states, a critical review, *J. Phys.: Complexity* **2**, 032001 (2021).
- [7] G. C. Sethia, A. Sen, and G. L. Johnston, Amplitude-mediated chimera states, *Phys. Rev. E* **88**, 042917 (2013).
- [8] Y. Kuramoto, *Chemical Oscillations, Waves, and Turbulence*, Springer Series in Synergetics (Springer, Berlin, 1984), Vol. 19.
- [9] I. S. Aranson and L. Kramer, The world of the complex Ginzburg-Landau equation, *Rev. Mod. Phys.* **74**, 99 (2002).
- [10] M. Cross and H. Greenside, *Pattern Formation and Dynamics in Nonequilibrium Systems* (Cambridge University Press, Cambridge, 2009).
- [11] L. Schmidt, K. Schönleber, K. Krischer, and V. García-Morales, Coexistence of synchrony and incoherence in oscillatory media under nonlinear global coupling, *Chaos* **24**, 013102 (2014).
- [12] G. C. Sethia and A. Sen, Chimera States: The Existence Criteria Revisited, *Phys. Rev. Lett.* **112**, 144101 (2014).
- [13] C. R. Laing, Chimeras in networks with purely local coupling, *Phys. Rev. E* **92**, 050904(R) (2015).
- [14] M. R. Tinsley, S. Nkomo, and K. Showalter, Chimera and phase-cluster states in populations of coupled chemical oscillators, *Nat. Phys.* **8**, 662 (2012).
- [15] S. Nkomo, M. R. Tinsley, and K. Showalter, Chimera and chimera-like states in populations of nonlocally coupled homogeneous and heterogeneous chemical oscillators, *Chaos* **26**, 094826 (2016).
- [16] V. Vanag, L. Yang, M. Dolnik, A. Zhabotinsky, and I. Epstein, Oscillatory cluster patterns in a homogeneous chemical system with global feedback, *Nature (London)* **406**, 389391 (2000).
- [17] V. K. Vanag, A. M. Zhabotinsky, and I. R. Epstein, Pattern formation in the Belousov-Zhabotinsky reaction with photochemical global feedback, *J. Phys. Chem. A* **104**, 11566 (2000).
- [18] F. Mertens, R. Imbühl, and A. Mikhailov, Turbulence and standing waves in oscillatory chemical reactions with global coupling, *J. Chem. Phys.* **101**, 9903 (1994).
- [19] C. R. Laing and C. C. Chow, Stationary bumps in networks of spiking neurons, *Neural Comput.* **13**, 1473 (2001).
- [20] N. Rattenborg, C. Amlaner, and S. L. Lima, Behavioral, neurophysiological and evolutionary perspectives on unihemispheric sleep, *Neurosci. Biobehav. Rev.* **24**, 817 (2000).
- [21] D. Barkley and L. S. Tuckerman, Computational Study of Turbulent Laminar Patterns in Couette Flow, *Phys. Rev. Lett.* **94**, 014502 (2005).
- [22] Y. Duguet and P. Schlatter, Oblique Laminar-Turbulent Interfaces in Plane Shear Flows, *Phys. Rev. Lett.* **110**, 034502 (2013).
- [23] M. J. Panaggio and D. M. Abrams, Chimera states: Coexistence of coherence and incoherence in networks of coupled oscillators, *Nonlinearity* **28**, R67 (2015).
- [24] I. Miethe, V. García-Morales, and K. Krischer, Irregular Subharmonic Cluster Patterns in an Autonomous Photochemical Oscillator, *Phys. Rev. Lett.* **102**, 194101 (2009).
- [25] V. García-Morales, A. Orlov, and K. Krischer, Subharmonic phase clusters in the complex Ginzburg-Landau equation with nonlinear global coupling, *Phys. Rev. E* **82**, 065202(R) (2010).
- [26] S. W. Haugland, L. Schmidt, and K. Krischer, Self-organized alternating chimera states in oscillatory media, *Sci. Rep.* **5**, 9883 (2015).

- [27] I. Prigogine and R. Lefever, Symmetry Breaking Instabilities in Dissipative Systems. II, *J. Chem. Phys.* **48**, 1695 (1968).
- [28] G. Nicolis and I. Prigogine, *Self-Organization in Nonequilibrium Systems: From Dissipative Structures to Order through Fluctuations* (Wiley, New York, 1977).
- [29] A. M. Zhabotinsky, A history of chemical oscillations and waves, *Chaos* **1**, 379 (1991).
- [30] G. Nicolis, *Introduction to Nonlinear Science* (Cambridge University Press, Cambridge, 1995).
- [31] N. M. Krylov and N. N. Bogoliubov, *Introduction to Non-Linear Mechanics* (Princeton University Press, Princeton, 1949).
- [32] P. Kumar and G. Gangopadhyay, Energetic and entropic cost due to overlapping of Turing-Hopf instabilities in the presence of cross diffusion, *Phys. Rev. E* **101**, 042204 (2020).
- [33] S. Cox and P. Matthews, Exponential time differencing for stiff systems, *J. Comput. Phys.* **176**, 430 (2002).
- [34] R. Rao and M. Esposito, Nonequilibrium Thermodynamics of Chemical Reaction Networks: Wisdom from Stochastic Thermodynamics, *Phys. Rev. X* **6**, 041064 (2016).
- [35] G. Falasco, R. Rao, and M. Esposito, Information Thermodynamics of Turing Patterns, *Phys. Rev. Lett.* **121**, 108301 (2018).
- [36] I. Prigogine and R. Defay, *Chemical Thermodynamics* (Longmans, London, 1954).
- [37] R. A. Alberty, *Thermodynamics of Biochemical Reactions* (Wiley, Hoboken, 2003).
- [38] E. Fermi, *Thermodynamics* (Dover, New York, 1956).
- [39] H. S. Haraldsdóttir and R. M. T. Fleming, Identification of conserved moieties in metabolic networks by graph theoretical analysis of atom transition networks, *PLoS Comput. Biol.* **12**, e1004999 (2016).
- [40] H. S. Lawson, G. Holló, R. Horvath, H. Kitahata, and I. Lagzi, Chemical resonance, beats, and frequency locking in forced chemical oscillatory systems, *J. Phys. Chem. Lett.* **11**, 3014 (2020).
- [41] P. Welch, The use of fast Fourier transform for the estimation of power spectra: A method based on time averaging over short, modified periodograms, *IEEE Trans. Audio Electroacoust.* **15**, 70 (1967).
- [42] B. J. Gluckman, P. Marcq, J. Bridger, and J. P. Gollub, Time Averaging of Chaotic Spatiotemporal Wave Patterns, *Phys. Rev. Lett.* **71**, 2034 (1993).
- [43] D. Gabor, Theory of communication. Part 1: The analysis of information, *J. Inst. Electr. Eng.* **III 93**, 429 (1946).
- [44] M. Farge, Wavelet transforms and their applications to turbulence, *Annu. Rev. Fluid Mech.* **24**, 395 (1992).
- [45] J. G. Daugman, Uncertainty relation for resolution in space, spatial frequency, and orientation optimized by two-dimensional visual cortical filters, *J. Opt. Soc. Am. A* **2**, 1160 (1985).
- [46] D. M. Abrams and S. H. Strogatz, Chimera states in a ring of nonlocally coupled oscillators, *Int. J. Bifurcat. Chaos* **16**, 21 (2006).
- [47] I. Omelchenko, O. E. Omel'chenko, P. Hövel, and E. Schöll, When Nonlocal Coupling between Oscillators Becomes Stronger: Patched Synchrony or Multichimera States, *Phys. Rev. Lett.* **110**, 224101 (2013).
- [48] T. Kotwal, X. Jiang, and D. M. Abrams, Connecting the Kuramoto Model and the Chimera State, *Phys. Rev. Lett.* **119**, 264101 (2017).
- [49] F. P. Kemeth, S. W. Haugland, L. Schmidt, I. G. Kevrekidis, and K. Krischer, A classification scheme for chimera states, *Chaos* **26**, 094815 (2016).
- [50] K. Bansal, J. O. Garcia, S. H. Tompson, T. Verstynen, J. M. Vettel, and S. F. Muldoon, Cognitive chimera states in human brain networks, *Sci. Adv.* **5**, eaau8535 (2019).
- [51] I. Daubechies, The wavelet transform, time-frequency localization and signal analysis, *IEEE Trans. Inf. Theory* **36**, 961 (1990).
- [52] T. S. Lee, Image representation using 2D Gabor wavelets, *IEEE Trans. Pattern Anal. Mach. Intell.* **18**, 959 (1996).
- [53] J. G. Daugman, Two-dimensional spectral analysis of cortical receptive field profiles, *Vision Res.* **20**, 847 (1980).